Available online at www.sciencedirect.com
SCIENCE DIRECT®

Journal of the European Ceramic Society 23 (2003) 1723–1733
www.elsevier.com/locate/jeurceramsoc

Finite element simulation of straight plunge grinding for advanced ceramics

Tze-jer Chuang*, Said Jahanmir, Hai C. Tang

National Institute of Standards and Technology, Gaithersburg, MD 20899 USA

Received 23 April 2002; received in revised form 7 October 2002; accepted 28 October 2002

Abstract

The objective of this work is to model the grinding forces and the associated stress and deformation fields generated in a ceramic workpiece during plunge surface grinding. A two-dimensional finite element model is constructed with the grinding parameters and the mechanical properties of the workpiece as input variables. The size of the geometric model is several times larger than the size of the cutting zone, using approximately 5200 rectangular solid elements with a finer mesh in the cutting zone and with fixed remote boundaries. The loading in the cutting zone is imposed by displacement vectors proportional to the local undeformed chip thickness, which is a function of grinding parameters. For a given set of inputs, the model predicts the normal and tangential forces generated by the grinding wheel, as well as the deformation and the stress fields within the workpiece. As an example, the simulation is applied to a silicon nitride workpiece. Analysis of the stress fields developed in this material suggests that shear failure within the cutting zone is the dominant mode of subsurface failure, which could lead to the formation of shear micro- cracks at the grain interfaces. The depth of the subsurface shear failure zone increases with an increase in maximum undeformed chip thickness or the wheel depth of cut. The resulting local grinding force vectors, maximum stresses and damage zone sizes are predicted as a function of maximum undeformed chip thickness (or the wheel depth of cut).
Published by Elsevier Science Ltd.

Keywords: Finite element methods; Grinding; Horizontal surface grinding; Plunge grinding; Simulation

1. Introduction

The cost of machining for advanced ceramic parts frequently dominates the overall production costs. Reducing the cost or increasing the yield *without* degrading performance of the finished workpiece is a critical issue in determining whether ceramics can be used in many applications. To tackle this problem, much effort has been devoted to the collection of data on the effects of machining parameters on the process outputs (see, Refs. 1 and 2). Because of numerous variables involved in grinding, an empirical approach is time-consuming and difficult to sort out the contribution of each parameter.

The present paper is a first step in developing a model for horizontal surface plunge grinding. It is generally believed that the mechanism of material removal or chip formation is due to cut and shear of the traveling grits by dynamic indentation.[3] This type of sharp cutting inadvertently introduces surface and sub-surface damage as well as residual stresses in the ground piece which, in turn, degrade the performance of the work in service.[3,4] Evidently cost- effectiveness demands high yield which requires higher material removal rate, resulting in a higher degree of damage and ultimately inferior performance of the finished part. To strike a balance between cost effectiveness and quality of the ground product is the main challenge that theoretical work can help to meet.

The primary objective of the present paper is to model the deformation and stress fields produced in the workpiece during surface grinding as a function of grinding parameters. Once the extent and nature of surface and subsurface damage is quantified, the strength degradation, if any, can be assessed. In order to achieve this goal, the finite element approach will be adopted, due to the complexity in geometry. The use of finite element techniques in solving the machining problems has been applied to the chip formation processes in metal cutting,[5,6] to

* Corresponding author.

0955-2219/03/$ - see front matter Published by Elsevier Science Ltd.
PII: S0955-2219(02)00409-0

sheet metal forming,[7] and to surface generation during rough machining.[8] The subject of investigation focuses on the metal chip behavior which is ductile. Metal plasticity is the major constitutive law adopted to tackle this class of problems.[5] Recently, Berth applies the techniques to model the grinding wheel's thermo-mechanical behavior during high speed rotation in grinding.[7] It is fair to say that application of the techniques to the grinding problems, particularly the case of grinding brittle ceramics, appears to be scarce in the machining literature. Using a finite element technique to simulate the effects of the cutting action of each individual grit, we will focus attention on a specific grit and assess the boundary conditions imposed due to this action.

After the finite element model is constructed, the prediction of forces as a function of depth of cut can be checked against experimental measurements for fixed values of grinding parameters. Once the verification is made, the model can be extended to predict other functional relationships with other grinding parameters, thereby reducing the need for time-consuming empirical experimental work.

2. Mechanics of surface grinding

The geometry of straight surface plunge grinding is shown in Fig. 1. In this operation, the workpiece is moved at a relative constant table speed V_w against a rotating wheel, which has a constant peripheral speed V_s. A wheel depth of cut a is imposed on the workpiece by the grinding wheel, whereby a layer of material with thickness a is removed from the surface as the wheel traverses over the entire length of the workpiece. Small chips are removed from the grinding zone mainly as a result of contacts made between the workpiece and the abrasive grits located at the periphery of the wheel rim. A coolant or grinding fluid is usually applied to the grinding zone to remove the chips and to control the workpiece temperature. The thermal aspects of the grinding problem are ignored to simplify the present analysis. A particular grit on the rotating wheel enters the cutting zone at a tangential velocity V_s and follows a parabolic curve (if depth is small, which it is),[4] which can be mathematically described as

$$y = \frac{x^2}{D} \tag{1}$$

where a Cartesian coordinate system is established with the origin set at the grit entering point of the cutting zone [see Fig. 1(b)]. In this equation, D is the effective wheel diameter defined by

$$D = d_w \times (1 \pm V_w/V_s)^2 \tag{2}$$

where d_w is the wheel diameter. The plus sign is used for the case of up-grinding (i.e. V_s in the opposite direction of V_w) and the minus sign is used for down-grinding (i.e. V_s in the same direction to V_w). The parabolic trace described by Eq. (1) will end at the point ($x = L$, $y = a$) where the grit leaves the workpiece surface. Note that here, a is the wheel depth of cut imposed by the grinding wheel and that the geometric contact length L can be described as

$$L = (a \times D)^{1/2} \tag{3}$$

Therefore, Eq. (1), which is valid in the range $0 \leqslant x \leqslant L$ and $0 \leqslant y \leqslant a$ describes the initial geometry of the grinding zone from the origin (0,0) to the exit point (L, a). Please refer to Fig. 1(b) for the schematic sketch for the grinding zone.

As the grit travels along the parabolic path, the local chip thickness $h(x)$ increases from zero at the origin to the maximum value, often referred to as the maximum undeformed chip thickness, h_m at the end point (L,a) according to kinematic considerations:[4]

$$h_m = \sqrt{\frac{5}{C \times S}\left(\frac{V_w}{V_s}\right)\sqrt{\frac{a}{D}}} \tag{4a}$$

where C is the number of cutting grits per unit area of the wheel surface and S is a chip shape factor. Alternatively, h_m can be shown to relate to a through the following equation:[6]

$$h_m = 1.26 \times \left[\frac{\pi d^3 \tan\gamma}{6V_f}\left(\frac{V_w}{V_s}\right)\sqrt{\frac{a}{D}}\right]^{1/3} \tag{4b}$$

where d is the grain size, 2γ is the vertex angle of the grain tip (average value is about 75°), V_f is the volume fraction of the abrasive grains. At any position along the cutting zone, the undeformed chip thickness $h(x)$ can be interpolated by the two apparent end points at (0,0) and at (L, a). That is, at the origin $h(x = 0) = 0$ and at the grit exit point $h(x = L) = h_m$. Therefore, $h(x)$ can be written as

$$h(x) = h_m \times \left(\frac{x}{L}\right)^2 \tag{5}$$

During grinding, as the grit follows the path described by Eq. (1), unknown, a priori up to a point, local forces are imposed on the work surface, which, in turn, generates a stress field within the workpiece underneath the grinding zone. When the resulting stresses exceed a threshold value (e.g. the fracture strength of the workpiece material), microfracture could take place, and a surface or subsurface damage zone will likely be formed. In this paper, an approximate numerical solution based on finite element method is used to quantify the grinding forces imposed on the workpiece and the associated stress and deformation fields generated in the workpiece.

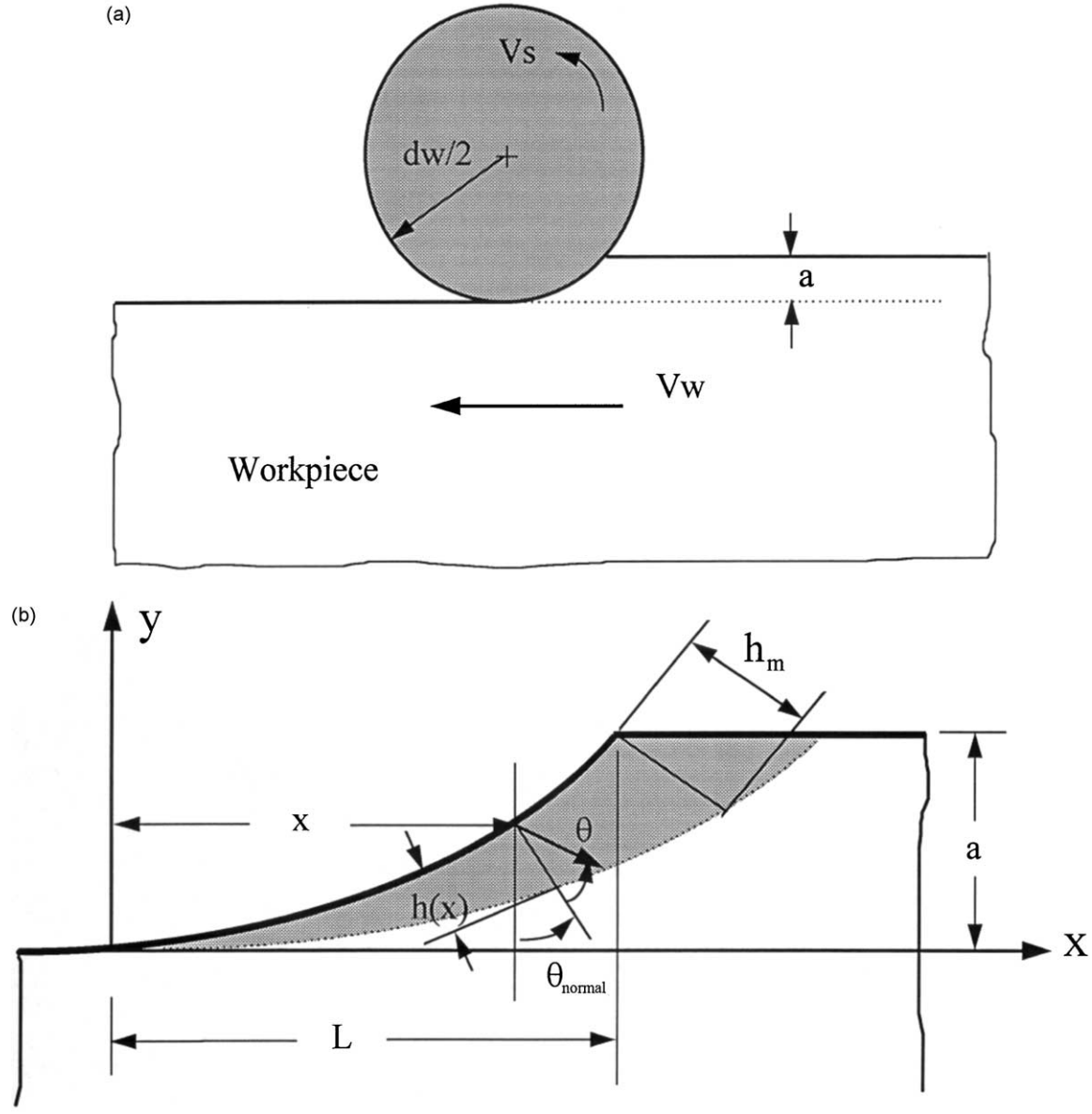

Fig. 1. (a) Schematic sketch of a typical straight plunge horizontal surface grinding operation. Important grinding parameters labeled here include: downfeed (or wheel depth of cut) a; table speed V_w; wheel speed V_s: wheel diameter d_w. Other important parameter such as wheel specifications are not shown; (b) a blow-up of the grinding zone, showing the relationship of the imposed displacement vector and normal vector in the Cartesian coordinate system.

3. Finite element model

The finite element method is a versatile and powerful tool for obtaining approximate solutions to mechanics problems associated with non-uniform stress distributions in geometrically complex shapes, where analytical techniques are either too difficult or often impossible to obtain. A general purpose, commercially available finite element program—ANSYS (certain commercial equipments, instruments, or materials are identified in this paper to foster understanding. Such identification does not imply recommendation or endorsement by the National Institute of Standards and Technology, nor does it imply that the equipment or software identified are necessarily the best available for the purpose), as implemented in an Unix operating system was used. One advantage of ANSYS is that it allows a parametric study, in which various solutions can be acquired for a variety of variables without the need to reconstruct the model manually when the values of the variables are changed. This feature is suitable for the present work.

3.1. Mesh design

The workpiece is regarded as a two-dimensional semi-infinite body. The overall dimension of the geometric

model is selected such that the length (in the x-direction) and the width (in the y-direction) are much larger than the size of the grinding zone. According to St.Venant's principle, in the theory of elasticity (see e.g. Refs. 9 and 10), the stresses at large distances from the point of load application must diminish. Thus, the remote boundaries were selected at $x=-0.5\times L$ and $x=2\times L$ in the horizontal direction, and $y=10\times a$ in the vertical direction. The overall dimension of the geometric model is accordingly flexible and depends on L and a, which in turn are functions of the grinding parameters. However, during the parametric study, we found that the width of the model must be kept fixed to obtain a meaningful comparison between different grinding conditions. This is because in the case of displacement boundary value problems, the boundary forces generated are proportional to the boundary elastic strains, which are inversely proportional to the depth of the model. For example, in analogy to the case of indentation problem, if the depth of the model is allowed to vary, then a comparison cannot be made. Therefore, a fixed vertical dimension of 2 mm was used, regardless of grinding conditions; whereas the horizontal dimension was varied from 5 mm to 10 mm depending on L, or grinding conditions.

Although the material removal process in ceramics involves small scale plastic deformation as discussed previously in the Introduction, an elastic solution is used in this preliminary analysis. Two-dimensional plate elements with four corner nodes were used since such an element is usually adequate for linear elastic problems. Rectangular elements were used on the two sides of the grinding zone (Fig. 2). Both the width (y-direction) and the length (x-direction) of these elements were gradually increased as the distance from the edges of the grinding zone were increased. Within the grinding zone, the elements had two straight edges (along the y-direction) and curved surfaces (along the x-direction). To accommodate the parabolic shape of the grinding zone, Eq. (1) was used for the outer surface of the elements in the first layer. The curvature of the elements was gradually relaxed as the interior of the semi-infinite plate was approached. In order to minimize the computation time and at the same time obtain accurate values for the stresses in the grinding zone, a small width was selected for the elements near the top surface. The width was gradually increased as the distance from the grinding zone was increased, but the length was kept constant. Fig. 2 shows a typical mesh design for a particular grinding condition. A total of 5200 elements and 5371 nodal points are included in the model shown in Fig. 2.

3.2. Boundary conditions

Since the remote boundaries on either side and the bottom of the geometric model are located far away from the grinding zone, the displacement vectors are assumed to be zero. The top surface of the workpiece is assumed to be free of tractions outside the grinding zone. During grinding, a single grit follows the path described by Eq. (5) and the material enclosed between the two paths described by Eqs. (1) and (5) is removed. Modeling of the chip formation process in ceramics is very complex, since chip formation in these brittle materials follows a fragmentation process, unlike metal cutting where a continuous or a semicontinuous chip geometry can be assumed. Therefore, in the present analysis a displacement boundary condition is imposed within the grinding zone. It is assumed that the abrasive grits on the wheel apply a set of displacement vectors with the magnitude equal to the undeformed local chip thickness $h(x)$ as described by Eq. (5). During initial attempts, the imposed displacement vectors were applied horizontally in the x-direction. However, the resulting normal and tangential forces were found to be unrealistically too large and the ratio of the tangential force to normal force to be too much larger than unity. Since the ratio of tangential to normal grinding force for ceramic is on the order of 0.2–0.3 different approaches were tried to obtain more realistic ratios through the simulations. The best solution was obtained when the direction of the local displacement vector was allowed to vary gradually from the entrance to the exit point in the grinding zone. If we define θ_{normal} as the angle between the normal vector and the vertical y-axis, such that $\theta_{\text{normal}}=\arctan(2\times/D)$, then the angle θ measured counter-clockwise from the normal vector defines the direction of the local displacement vector $\mathbf{u}$ [see Fig. 1(b)]. The total angle $(\theta+\theta_{\text{normal}})$ is assumed to vary linearly from zero at $x=0$ to $\pi/2$ at $x=L$. Therefore, the applied displacements in x and y directions become

$$U_x(x) = h(x)\cdot\sin(\theta+\theta_{\text{normal}}) \tag{6}$$

$$U_y(x) = h(x)\cdot\cos(\theta+\theta_{\text{normal}}) \tag{7}$$

3.3. Constitutive properties of the work

The chip formation process in ceramic grinding involves not only elastic deformations but also irreversible plastic deformation and microfracture. In a comprehensive simulation, one must also model the processes of heat generation and thermal energy transfer. However, in the present work, we restrict our effort to examining the effects of loading forces to see how the stresses will be generated and to further determine the propensity for the formation of subsurface microfractures. Thus, unloading and thermal issues are neglected in this preliminary study. The semi-infinite plane of the ceramic polycrystalline workpiece is assumed to be homogeneous and isotropic. It is further assumed that during loading, the material follows a linear elastic behavior up to the point of failure without plastic

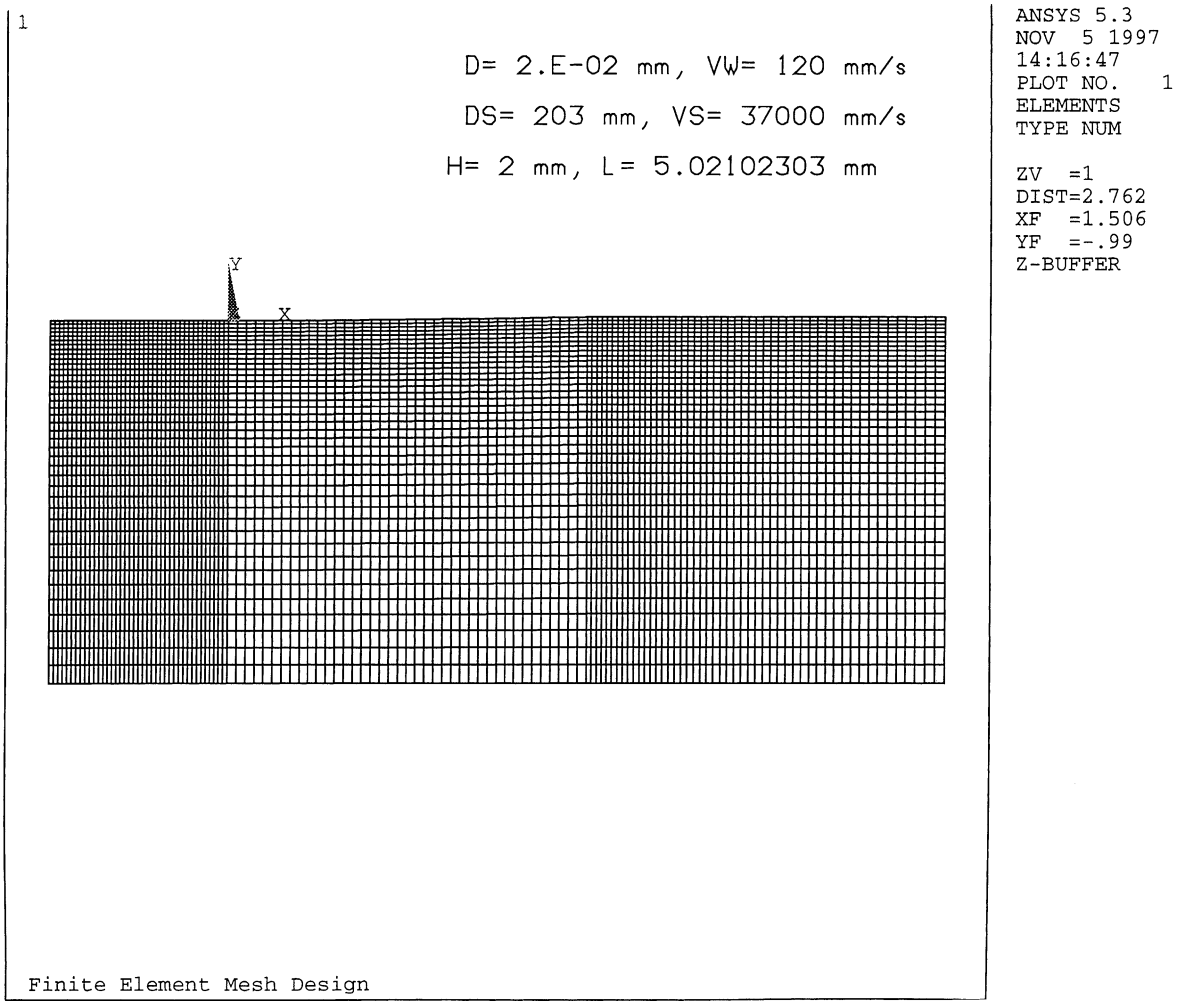

Fig. 2. Mesh design for the proposed finite element model. The model size is fixed at 2 mm in depth and about 5 mm wide depending on the amount of downfeed. The origin of the coordinate system is set at the beginning of the cutting zone. Note that finer meshes are constructed around the cutting zone.

yielding. Therefore, only Young's modulus E and Poisson's ratio ν are required for the analysis. In this simulation, we used $E = 300$ GPa and $\nu = 0.2$ as typical values for a sintered silicon nitride with a flexural strength value of about 600 MPa and a hardness of 14 GPa.[16] The hardness and strength values are not used in the elastic analysis but they are useful indicators of the deformation and fracture properties and will be referred to for interpretation of the simulation results.

3.4. Simulation procedure

Given a set of grinding parameters, the simulation procedure begins by computing the length of the grinding zone L and the effective wheel diameter D so that the profile of the grinding zone as depicted by Eq. (1) can be determined. The grinding parameters needed for the simulation include: wheel diameter d_w, table speed V_w, wheel speed V_s, wheel depth of cut a, wheel surface grit density C and grit shape factor S based on Eq. (4a) or grain size, volume fraction and tip angle based on Eq. (4b). Once the profile of the grinding zone is determined and the dimensions of the geometric model are defined, the mesh design demonstrated by Fig. 2 is then constructed. A typical two-dimensional finite element model constructed for a parametric study consists of some 1800 rectangular elastic elements with a total of about 3600 degrees of freedom for the unknown displacements U_x and U_y. The second step is to set up the displacement boundary conditions at the remote boundaries, the stress boundary conditions on the top surface outside the grinding zone, and the displacement boundary condition within the grinding zone. With the imposed boundary conditions a solution is sought for the boundary forces (i.e. forces exerted on the work surface by the grinding wheel) and the stress and displacement fields inside the workpiece resulting from the simulated grinding action.

In this simulation, the following grinding parameters were used to allow a comparison with the grinding studies in which grinding forces data and information

on subsurface damage structure are available (see, e.g. Ref. 12). The wheel speed was set at 37 m/s and the table speed at 0.12 m/s. The grinding wheel diameter d_w was set at 203 mm. The wheel surface grit density C was 10 and a grit shape factor S was assumed to be equal to 6 for Eq. (4a); and $V_f = 25$ vol.%, $\gamma = 35°$, $d = 0.5$ μm for Eq. (4b). While these parameters were kept constant, the maximum undeformed chip thickness h_m were varied from 0.31 to 0.62 μm based on Eqs. (4) for a ranges from 0.24 to 60 μm. The force is expressed in the unit of newton (N), the length in millimeter (mm), and accordingly the stress is in megapascal (MPa).

3.5. Simulation results

3.5.1. Boundary force solutions

Fig. 3 is a plot of the traction force distribution calculated at the surrounding boundary for a depth of cut equal to 20 μm. It can be shown that summation of all normal forces vanishes and the equilibrium conditions are satisfied. This is also true for the tangential forces. Furthermore, it can be seen that the remote boundary forces are negligible, indicating the dimensions of the model are sufficiently large to adequately simulate the physical process of grinding. The calculated forces in the grinding zone can be interpreted as being the grinding forces. There are 41 nodal points distributed along the grinding arc. Hence there are 41 traction forces resulted from the boundary force solutions. A summation of the forces at the nodes can be interpreted as the force exerted on the wheel during grinding. For the particular case, $h_m = 0.52$ μm, in Fig. 3, the normal grinding force $F_y = 11.28$ N/mm downward, and the tangential grinding force $F_x = 3.12$ N/mm to the right in the horizontal direction. It should be noted that a conversion factor should be made to reflect the fact that the solutions are based on plane-strain conditions per unit thickness (i.e. 1 mm) of the work in the z-direction. The magnitude and the ratio of these forces agree with the experimental results obtained in Ref. 16.

3.5.2. Stress solutions

All stress components, including normal stress, shear stress, three principal stresses and equivalent stress were

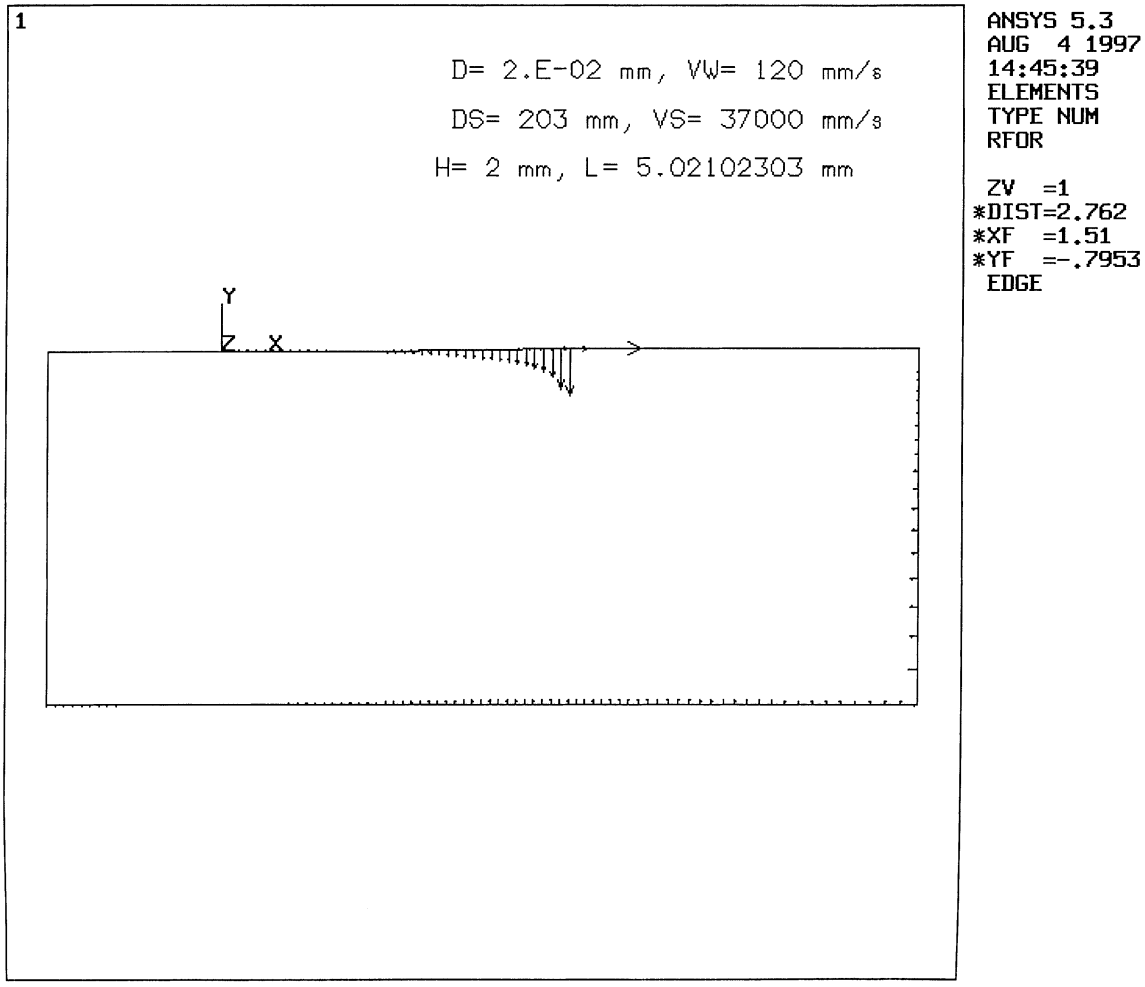

Fig. 3. Vectorial illustration of the boundary force solutions obtained for the following set of grinding parameters: $d_w = 20.3$ cm; $h_m = 0.520$ μm; $V_w = 12$ cm/s; $V_s = 37$ m/s.

obtained as a result of the simulation for different maximum undeformed chip thickness. Of particular importance are the critical tensile stress, the maximum shear stress, and the maximum compressive stress. The contour plot in Fig. 4(A) shows the distribution of the first principal stresses or the tensile stress field for a maximum undeformed chip thickness equal to 0.52 μm. The tensile stresses, as shown in Fig. 4(B) which is a blow-up of the cutting zone, range from zero to approximately 323 MPa with the maximum occurring at the grit exit point ($x = L$). The magnitudes of the tensile stresses are large only underneath the grinding zone and diminish rapidly as the interior is approached. The maximum tensile stress ranged from 500 to 400 MPa as the maximum undeformed chip thickness was increased from 0.31 to 0.62 μm.

The shear stress field for a maximum undeformed chip thickness equal to 0.52 μm is shown in Fig. 5(A). In comparison with the tensile stresses, the resulting shear stresses are significantly larger in magnitude, especially near the grit exit point. The shear stress contours are centered at the grit exit point, and skewed to the right of the grinding zone. In order to show the details, the local region underneath the cutting zone is enlarged in Fig. 5(B). As can be seen, the maximum shear stress value for this particular example is 642 MPa. The maximum values always occurred at the exit point and ranged from 710 to 700 MPa when the maximum undeformed chip thickness was increased from 0.31 to 0.52 μm.

The shear strength of sintered silicon nitride is approximately 250 MPa.[13] The solution as suggested by the contour plot in Fig. 5 indicates that a damage zone of the size of ≈70 μm is likely to form in the subsurface region which cannot be removed by the grinding process because they are located below $y = 0$. This prediction has a strong implication which will be discussed in the following section.

The compressive stress (i.e. the third principal stress) field underneath the grinding zone is given in Fig. 6(A).

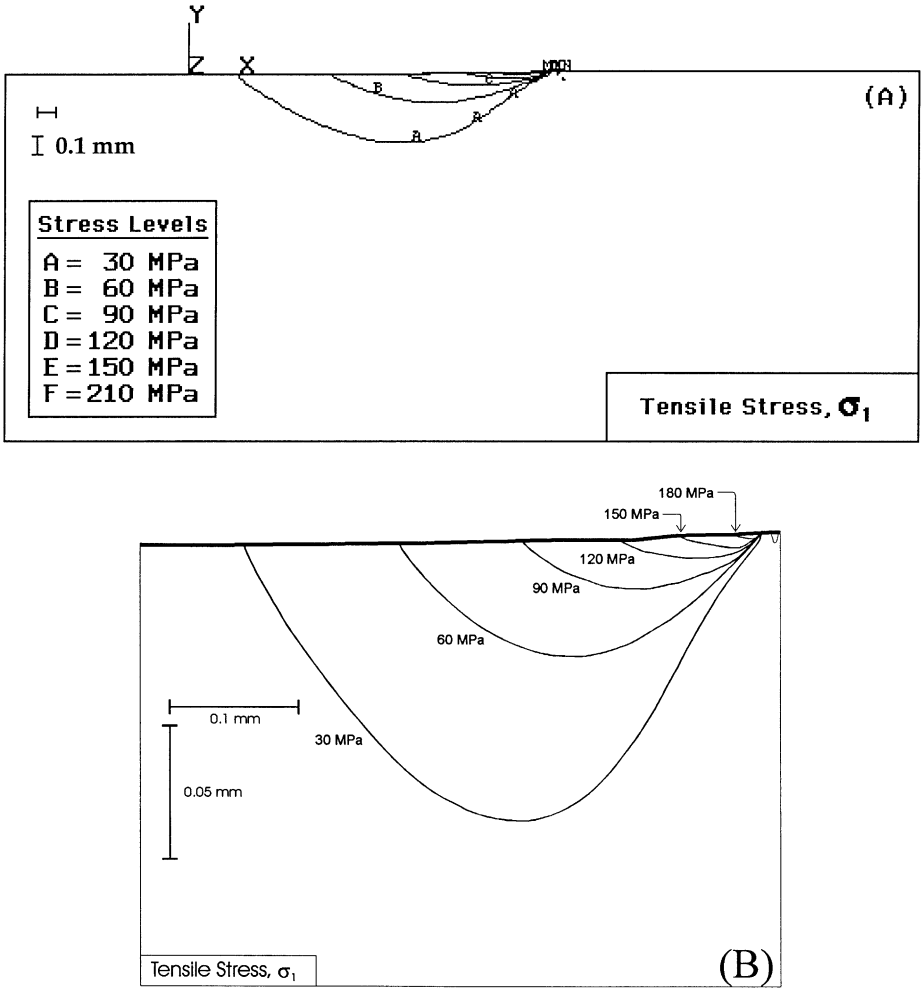

Fig. 4. (A) Contour plot of the tensile stress (or the first principle stress) solution for the same parameters as Fig. 3. (B) The blow-up of the critical zone. The maximum stress of 275 MPa is located at the other end of the cutting zone where the undeformed chip thickness is also maximum. Since it occurs above the remove zone, this type of stress should not create residual damage for the finished product.

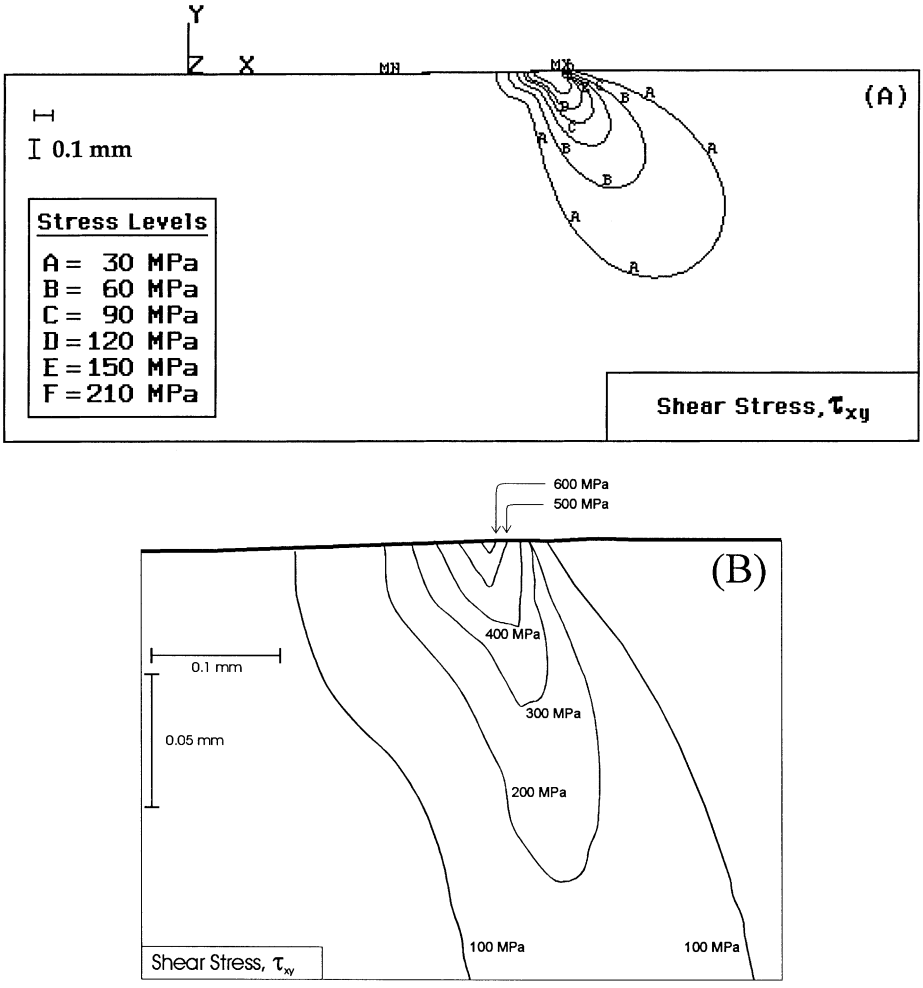

Fig. 5. (A) Contour plot of the shear stress solution for the same parameters as given in Fig. 3. (B) Detailed plot of the critical area. Although the maximum shear stress of 478 MPa also occurs at the same location as tensile stress field, a subsurface damage zone, however, is expected to form ahead of the cutting zone. The zone size is estimated in the range of 50–200 μm, depending on the shear strength of the workpiece.

As expected the values of compressive stresses are much larger than the tensile or shear stress values. The maximum compressive stress for this particular example is 1.85 GPa and is also located at the grit exit point [see Fig. 6(B)]. The maximum compressive stress ranged from 2.50 to 1.85 GPa as the maximum undeformed chip thickness was increased from 0.31 to 0.52 μm (Fig. 7).

The effect of maximum undeformed chip thickness on the magnitude of maximum tensile, compressive, and shear stresses developed during grinding are shown in Fig. 7. Although the position of these maximum values were not the same, they were located in the neighborhood of the exit point ($x=L$, $y=a$). One interesting observation is that as the maximum undeformed chip thickness increases, the maximum stresses decay and reach a constant value at 1.85 GPa for compression, 700 MPa for shear and 400 MPa for tension. Intuitively, one may expect the maximum stresses to increase monotonically with increasing h_m. However, the finite element solutions indicate that as the depth of cut is increased, the maximum tensile stresses do not change much. Instead the region associated with the maximum values is enlarged, as the underlying material supports the stresses. This is shown in Fig. 8, where the depth measured from (L, a) corresponding to one half of the maximum stress (an arbitrary value) is plotted as a function of the maximum undeformed chip thickness.

It is important to note that the maximum values of the stress tensor may be influenced by the singular points. Thus, the values are sensitive to the mesh design: changing the element sizes near the cutting zone will affect the solution of the maximum stresses, but not the underlying stress field.

With the availability of the stress field solutions as given in the previous section, we can roughly estimated the extent of possible damage zone that could be developed by assuming the stresses in the zone exceed the materials strength. Strictly speaking, of course, the true damage zone can only be ascertained by a nonlinear analysis with incremental loading steps, because as the first bond rupture when the stress over there exceeds its

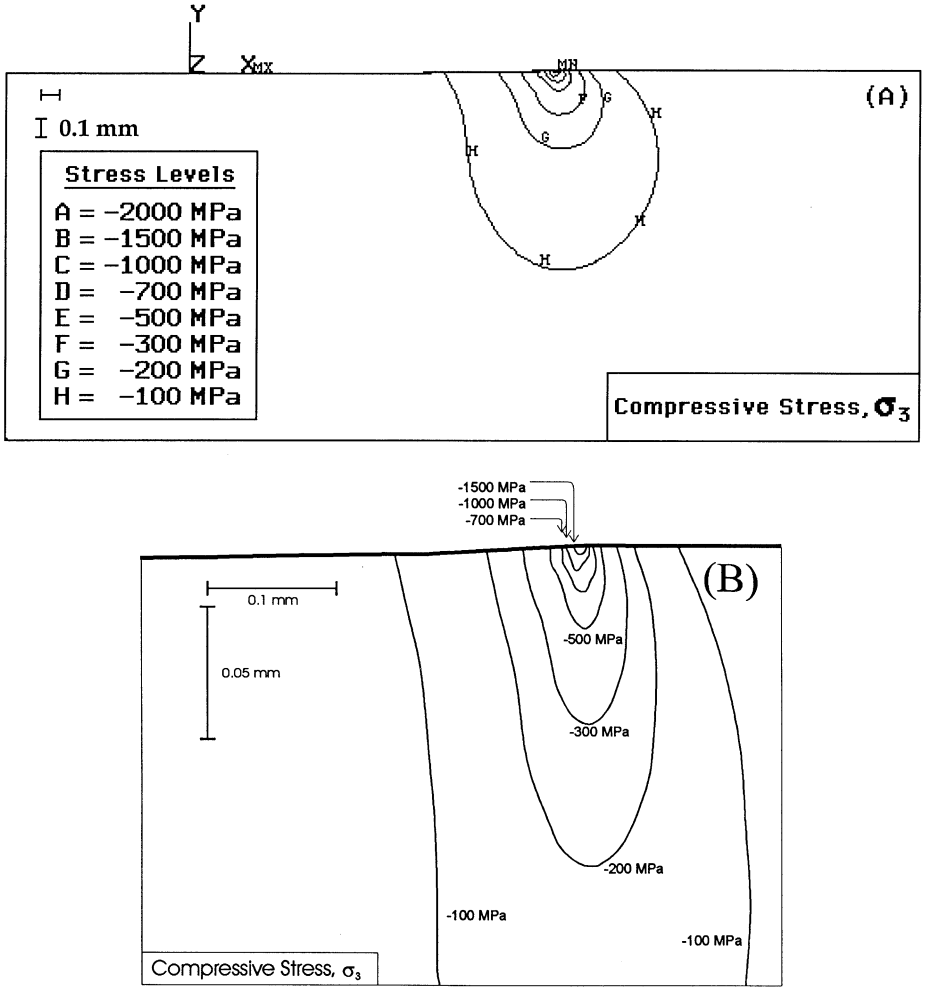

Fig. 6. (A) Compressive stress field developed as given by the third principal stresses in contour plot; the grinding parameters used are the same as in Figs. 4 and 5. (B) The blow- up of the critical area.

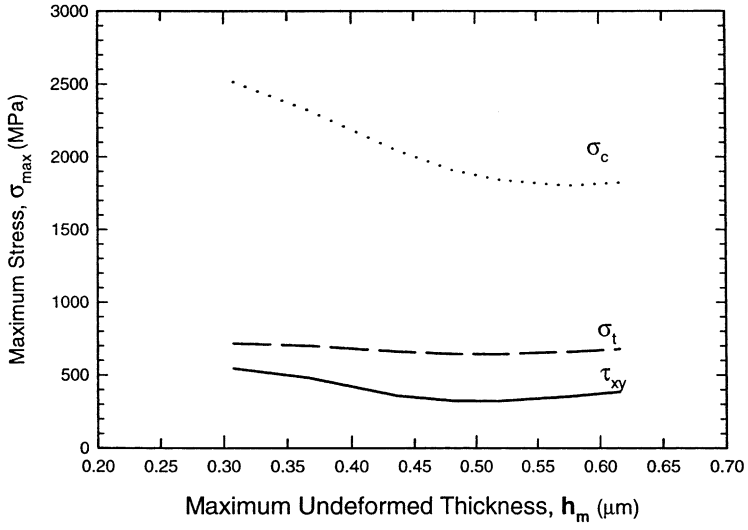

Fig. 7. Maximum stresses developed as a function of the maximum undeformed chip thickness for the same set of grinding parameters.

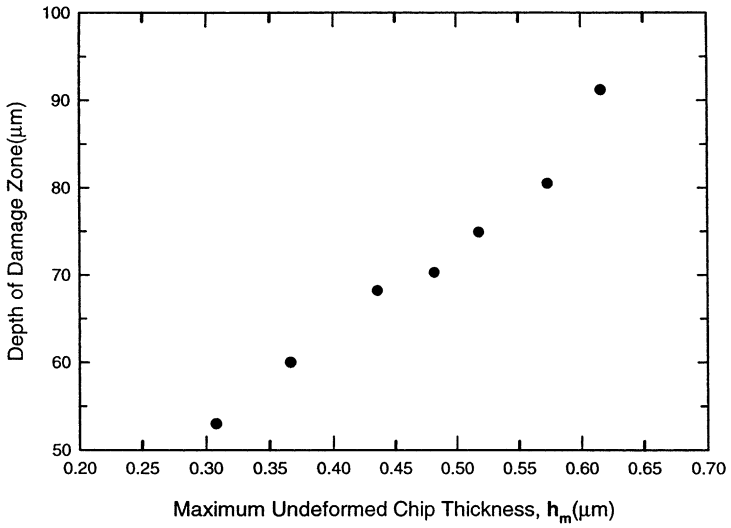

Fig. 8. Damage zone sizes predicted as a function of the maximum undeformed chip thickness. The damage is controlled by the shear stresses developed during grinding.

strength, the load can no longer be carried by the broken bond and it must be redistributed to the surrounding unruptured bonds. A new stress analysis is required for this new configuration until all stresses within the body lie below the materials strengths. Realistically this will give a lower bound solution. For the present paper, we assume the load did not redistribute, and the boundary of the damage zone has a stress value equal to the strength of the material. Furthermore, due to the nature of the brittle ceramics, the controlling stress for damage development as discussed in the previous section is the shear component of the stress tensor. Fig. 8 plots the damage zone size as measured in the vertical direction below $y=0$ due to shear stress as a function of the grit depth of cut, a in μm.

For example, when the maximum undeformed chip thickness is set at 0.52 μm, the predicted damage zone size would be 75 μm (Fig. 8). It is further observed that the functional relationship between damage zone and maximum undeformed chip thickness can be described as quadratic with a threshold at $h_m=0.32$ μm below which there will be no damage developed. This level is consistent with the predicted ductile/brittle transition mode predicted for this material.[14]

4. Discussion

The surface plunge grinding operation is a very complex process. It involves the moving wheel, the workpiece and the interactions between the two. The present paper deals only with global simulation of the grinding actions imposed by the wheel on the workpiece, the resulting forces, and the stresses generated in the work, especially beneath the grinding zone. The simulation results seem to agree well with the force data collected on a class of silicon nitride ceramics. The usefulness of this simulation is that it can perform systematic *virtual* experiments on the *computer* for examining the effects of a specific grinding parameter on the final status of the finished part. In this way, the empirical method of performing actual measurements in a *laboratory*, commonly adopted in the machining community, which is usually a time-consuming and labor intensive effort, can be reduced dramatically to a bare minimum.

There are, however, some major important issues that the present paper does not address. First, the model implies a steady state solution. Also, the simulation does not take into account the material removal process and the post rupture behavior. Thus, the model is only capable of predicting the size of the *potential* damage zone along the grinding surface. A real damage developed and the associated residual stress field solutions, as discussed before, must await a full nonlinear irreversible analysis of loading and unloading, in conjunction with implementing an elastic/damage constitutive law of the material property, together with element manipulations with element-death-and-birth feature to simulate material removal. We leave this interesting subject for future research.

Secondly, grinding is a highly dynamic event, involving high velocity impact, indentation or cutting, plowing and churning of abrasive particles on the workpiece surface. The inertial effects maybe important as they can influence the dynamic strength and toughness of the work.[12–16] Moreover, during the cutting, a substantial thermal energy is produced which enhances the temperature field in the cutting zone, thereby affecting the energy transfer and chip formation processes. Finally, as the coolant is applied to reduce the temperature of the grinding surface, chemical reactions between the fluid and the solid workpiece are promoted in the elevated temperature environment. This may alter the surface

property of the work, which, in turn, changes the tribological behavior of the work, and thus its machinability. Those issues are important but are not addressed in the present work. They certainly do deserve our attention for future research.

Last, but not least, an issue not addressed here is the topography of the grinding wheel which is also important, as the grit distribution is random and stochastic in nature. A finite element model on the grinding wheel was also proposed to study force and temperature distributions around the wheel rim.[7] Furthermore, the periphery of the wheel may not maintain a perfect circular shape, even if the wheel is fully trued. A viable approach to tackle this problem is based on a statistical method. For a given wheel specification, the average protrusion of the grits over the wheel baseline can be statistically determined.[17,18] A more rigorous approach of considering the collective action of *all* grits simultaneously acting on the arc of the interaction zone of the work surface will be presented elsewhere.[13,14] Both methods should yield similar results, if the simulation closely follows the real physical process of grinding. This information can then be used to solve the forces and damage produced based on the principle of indentation mechanics.[11,19] In this way, analytical expressions for the forces can be obtained in terms of the mechanical properties of the work, grinding parameters and wheel specifications. Nevertheless, both current method using finite element and micromechanic approaches just described seem to yield similar results which agree very well with the experimental measurements. In addition, Lee et al.,[20] and Fischer-Cripps and Lawn.[21] recently performed microindentation experiment on a silicon nitride substrate and observed from TEM micrographs that the damage underneath the indenter is predominately in the form of micro shear cracks at grain interfaces. This observation is consistent with the present simulation results which indicate that the potential subsurface damage should be triggered by the resulting shear stresses.

Acknowledgements

This work was supported by the Ceramic Machining Program of the National Institute of Standards and Technology. The authors are grateful to G. Quinn for many helpful discussions; and to W. Luecke and M. Kaufman for the preparation of Figs. 4–6.

References

1. Jahanmir, S., ed., *Machining of Advanced Materials. Proc. of the Int. Conf. on Machining of Advanced Materials, NIST Special Publication 487*. US Government Printing Office, Washington, DC, 1993.
2. Hockey, B. J., Rice, R. W., ed., *The Science of Ceramic Machining and Surface Finishing II. Proc. 2nd Symp. on Ceramic Machining and Surface Finishing, NBS Special Publication 562*. US Government Printing Office, Washington, DC, 1979.
3. Shaw, M. C., *Principles of Abrasive Processing*. Clarendon Press, Oxford, UK, 1996.
4. Malkin, S., *Grinding Technology—Theory and Applications of Machining with Abrasives*. Halsted Press, John Wiley and Sons, New York, NY, 1989.
5. Marusich, T. D. and Ortiz, M., Simulation of chip formation in high speed machining. In *Machining of Advanced Materials AMD Vol. 208/MD Vol. 59*, ed. S. Jain and D. C. H. Yang. ASME, New York, NY, 1995, pp. 127–139.
6. Li, K. and Liao, T. W., Surface/subsurface damage and the failure strength of ground ceramics. *J. Mater. Proc. Technol.*, 1996, **57**, 207–220.
7. Chiu, W. C., Endres, W. J. and Thouless, M. D., Surface formation during rough machining of brittle materials with a geometrically defined tool. In *Proc. McNu'97, 1997 Joint ASME, ASCE and SES Summer Meeting, Northwestern University, Evanston, IL, 29 June–2 July*, 1997, p. 356.
8. Berth, C., Analysis and modeling of dynamic process in grinding. (in press).
9. Timoshenko, S. P. and Goodier, J. N., *Theory of Elasticity*, 3rd edn. McGraw-Hill Book Co, New York, NY, 1970.
10. Fung, Y. C., *Foundation of Solid Mechanics*. Prentice-Hall, Englewood Cliffs, NJ, 1965.
11. Xu, H. H. K., Jahanmir, S., Ives, L. K., Job, L. S. and Ritchie, K. T., Short-crack toughness and abrasive machining of silicon nitride. *J. Am. Ceram. Soc.*, 1996, **79**, 3055–3064.
12. Wachtman, J. B., *Mechanical Properties of Ceramics*. Wiley-Interscience, John Wiley & Sons, New York, NY, 1996.
13. Chuang, T.-J. and Jahanmir, S., A micromechanic force model for grinding advanced ceramics (in press).
14. Chuang, T.-J. and Jahanmir, S., On the ductile/brittle transition mode in grinding brittle materials (in press).
15. Davage, R. W., *Mechanical Behavior of Ceramics*. Cambridge University Press, New York, NY, 1979.
16. McColm, I. J., *Ceramic Hardness*. Plenum Press, New York, NY, 1990.
17. Koshy, P., *Electrical Discharge Diamond Grinding: Mechanism of Material Removal and Modeling*. PhD thesis, Indian Inst. Tech., Kanpur, India (1996).
18. Koshy, P., Jain, V. K. and Lal, G. K., A model for the topography of diamond grinding wheels. *Wear*, 1993, **169**, 237–242.
19. Subhash, G., Huang, Y. and Chandra, A., Mechanics of material removal in ceramic grinding: dynamic indentation investigations. In *Proc. McNu'97, 1997 Joint ASME, ASCE and SES Summer Meeting, Northwestern University, Evanston, IL, 29 June–2 July*, 1997.
20. Lee, S. K., Wuttiphan, S. and Lawn, B. R., Role of microstructure in hertzian contact damage in silicon nitride: I. Mechanical characterization. *J. Am. Ceram. Soc.*, 1997, **80**(9), 2367–2381.
21. Fischer-Cripps, A. C. and Lawn, B. R., Indentation stress–strain curves for "quasi-ductile" ceramics. *Acta Metall.*, 1996, **44**, 519–527.